AFRL-RZ-WP-TP-2010-2245

EXPERIMENTAL INVESTIGATION OF AIR AND METHANE INJECTION FROM IN-STREAM FUELING PYLONS (POSTPRINT)

Jason C. Doster and Paul I. King

Air Force Institute of Technology

Mark R. Gruber and Campbell D. Carter

Propulsion Sciences Branch
Aerospace Propulsion Division

Michael D. Ryan

Universal Technology Corporation

Kuang-Yu Hsu

Innovative Scientific Solutions, Inc.

JULY 2008

AIR FORCE RESEARCH LABORATORY
PROPULSION DIRECTORATE
WRIGHT-PATTERSON AIR FORCE BASE, OH 45433-7251
AIR FORCE MATERIEL COMMAND
UNITED STATES AIR FORCE

REPORT DOCUMENTATION PAGE

Form Approved
OMB No. 0704-0188

1. REPORT DATE *(DD-MM-YY)*	2. REPORT TYPE	3. DATES COVERED *(From - To)*
July 2008	Conference Paper Postprint	01 August 2007 – 21 July 2008

4. TITLE AND SUBTITLE	5a. CONTRACT NUMBER
EXPERIMENTAL INVESTIGATION OF AIR AND METHANE INJECTION FROM IN-STREAM FUELING PYLONS (POSTPRINT)	In-house
	5b. GRANT NUMBER
	5c. PROGRAM ELEMENT NUMBER 62203F

6. AUTHOR(S)	
Jason C. Doster and Paul I. King (Air Force Institute of Technology)	5d. PROJECT NUMBER 3012
Mark R. Gruber and Campbell D. Carter (AFRL/RZAS)	5e. TASK NUMBER AI
Michael D. Ryan (Universal Technology Corporation) Kuang-Yu Hsu (Innovative Scientific Solutions, Inc.)	5f. WORK UNIT NUMBER 3012AI00

7. PERFORMING ORGANIZATION NAME(S) AND ADDRESS(ES)		8. PERFORMING ORGANIZATION REPORT NUMBER
Air Force Institute of Technology (AFIT/ENY) 2950 Hobson Way Wright-Patterson Air Force Base, OH 45433-7765 --- Propulsion Sciences Branch (AFRL/RZAS) Aerospace Propulsion Division Air Force Research Laboratory, Propulsion Directorate Wright-Patterson Air Force Base, OH 45433-7251 Air Force Materiel Command, United States Air Force	Universal Technology Corporation Dayton, OH 45432 -- Innovative Scientific Solutions, Inc. Dayton, OH 45440	AFRL-RZ-WP-TP-2010-2245

9. SPONSORING/MONITORING AGENCY NAME(S) AND ADDRESS(ES)	10. SPONSORING/MONITORING AGENCY ACRONYM(S)
Air Force Research Laboratory Propulsion Directorate Wright-Patterson Air Force Base, OH 45433-7251 Air Force Materiel Command United States Air Force	AFRL/RZAS
	11. SPONSORING/MONITORING AGENCY REPORT NUMBER(S) AFRL-RZ-WP-TP-2010-2245

12. DISTRIBUTION/AVAILABILITY STATEMENT
Approved for public release; distribution unlimited.

13. SUPPLEMENTARY NOTES
Conference paper published in the *Proceedings of the 44th AIAA/ASME/SAE/ASEE Joint Propulsion Conference and Exhibit*, conference held July 21 - 23, 2008, in Hartford, CT. PA Case Number: AFIT PA 080635; Clearance Date: 19 June 2008. The U.S. Government is joint author of this work and has the right to use, modify, reproduce, release, perform, display, or disclose the work.

14. ABSTRACT

This paper covers experimental results for in-stream fuel injectors in a Mach number 1.95 airflow. Three fuel injection pylon configurations studied include a basic pylon, a ramp pylon, and an alternating wedge pylon. The first pylon is a baseline configuration. The latter two introduce streamwise vorticity into the flow to increase mixing action via their trailing edge geometries. A cold flow study with fuel injection is accomplished to compare the three pylons mixing capabilities and pressure losses. Three experimental techniques are used: aerothermal probing, Raman spectroscopy, and nitric-oxide planar laser induced fluorescence (NO-PLIF). Aerothermal probing and NO-PLIF are accomplished with air injection from the pylons, while Raman spectroscopy is accomplished with methane injection. The ramp and alternating wedge pylons show decisive increases in mixing capability compared with the basic pylon. They also exhibit a slight increase in total pressure loss compared with the basic pylon.

15. SUBJECT TERMS
Supersonic combustion, strut fuel injection, laser-based diagnostics, diode lasers, PLIF

16. SECURITY CLASSIFICATION OF:			17. LIMITATION OF ABSTRACT:	18. NUMBER OF PAGES	19a. NAME OF RESPONSIBLE PERSON (Monitor)
a. REPORT Unclassified	b. ABSTRACT Unclassified	c. THIS PAGE Unclassified	SAR	26	Mark R. Gruber 19b. TELEPHONE NUMBER *(Include Area Code)* N/A

Standard Form 298 (Rev. 8-98)
Prescribed by ANSI Std. Z39-18

Experimental Investigation of Air and Methane Injection from In-stream Fueling Pylons

Jason C. Doster[*] and Paul I. King[†]

Air Force Institute of Technology, Wright-Patterson Air Force Base, OH 45433

Mark R. Gruber[‡] and Campbell D. Carter[§]

Air Force Research Laboratory(AFRL/RZAS), Wright-Patterson Air Force Base, OH 45433

Michael D. Ryan[¶]

Universal Technology Corporation, Dayton, OH 45432

and

Kuang-Yu Hsu[‖]

Innovative Scientific Solutions, Inc., Dayton, OH, 45440

This paper covers experimental results for in-stream fuel injectors in a Mach number 1.95 airflow. Three fuel injection pylon configurations studied include a basic pylon, a ramp pylon, and an alternating wedge pylon. The first pylon is a baseline configuration. The latter two introduce streamwise vorticity into the flow to increase mixing action via their trailing edge geometries. A cold flow study with fuel injection is accomplished to compare the three pylons mixing capabilities and pressure losses. Three experimental techniques are used: aerothermal probing, Raman spectroscopy, and nitric-oxide planar laser induced fluorescence (NO-PLIF). Aerothermal probing and NO-PLIF are accomplished with air injection from the pylons, while Raman spectroscopy is accomplished with methane injection. The ramp and alternating wedge pylons show decisive increases in mixing capability compared with the basic pylon. They also exhibit a slight increase in total pressure loss compared with the basic pylon.

I.   Introduction

The Air Force Research Laboratory (AFRL) is currently studying low aspect ratio (circular or elliptical) scramjet combustor geometries as a practical, scalable design concept.[1,2] In order to distribute fuel uniformly in this combustor geometry an in-stream pylon fuel injector has been proposed.[3,4] Along with uniform fuel distribution, rapid mixing of the fuel and air is necessary to facilitate efficient combustion. Transverse fuel injection into a combustor airflow promotes rapid fuel/air mixing.[5] However, momentum from the fuel stream does not contribute to engine thrust in this case. Injecting fuel parallel to the combustor airflow augments engine thrust, but mixing is a concern.[6] To increase the mixing effectiveness of parallel injection, research on mixing geometries that create streamwise vortices in the combustor flow has shown promise. This has led to the concept of the hypermixer.[7] The two hypermixer geometries studied here are compression ramps and alternating wedges.[8–17] The two hypermixer geometries are incorporated onto the trailing edges of in-stream pylons, enhancing the mixing performance of the pylons. The two hypermixer pylons are compared to each other and a baseline pylon configuration with no hypermixer geometry on the trailing edge. Total pressure losses are also of concern, so the spreading and mixing capabilities of each pylon are considered relative to their pressure losses.

---

[*]PhD Candidate, Dept of Aeronautics & Astronautics, AIAA Member
[†]Professor, Dept of Aeronautics & Astronautics, AIAA Senior Member
[‡]Senior Aerospace Engineer, AIAA Associate Fellow
[§]Senior Aerospace Engineer, AIAA Associate Fellow
[¶]Research Scientist, AIAA Member
[‖]Senior Research Scientist, AIAA Senior Member

II. Pylon Configurations

The three pylon configurations are: the basic pylon (Fig. 1), the ramp pylon (Fig. 2), and the alternating wedge pylon (Fig. 3). The construction of each pylon incorporates a two-piece forward and aft area. The forward area contains a plenum common to all pylon configurations. The aft area contains a constant angled compression ramp on the basic pylon and a hypermixer geometry on the other two pylons. The mating of the two pieces results in tall/thin rectangular injection slots created by the difference in the inner width of the forward piece and the outer width of the aft piece. The common parameters for all pylons are: Height = 75 mm, Length = 103 mm, Frontal Blockage Area = 1215 mm^2, Fuel Port (Slot) Geometric Area = 57 mm^2, Front Wedge Half Angle = 14.7°, and Front Wedge Nose Radius = 1 mm.

The basic pylon configuration embodies the two fundamental fuel injection strategies of 1) maximizing fuel-air interface area by using a rectangular slot injector spanning a large percentage of the pylon height, and 2) injecting fuel upstream of the pylon aft area so fuel and air begin mixing prior to leaving the pylon surface. Figure 1 shows the basic pylon on a pedestal. The aft area of the basic pylon is a compression ramp at 10.6° (half angle) to the main airflow. The fueling slots operate at sonic conditions. A plenum in the forward area of the pylon provides fuel to the slots. This plenum is fed by a fuel tube at the bottom of the pylon connected to the pedestal. Fuel injection is accomplished from a backward facing step that protects the injectant from the main flow for a short distance prior to joining the main airflow around the pylon.
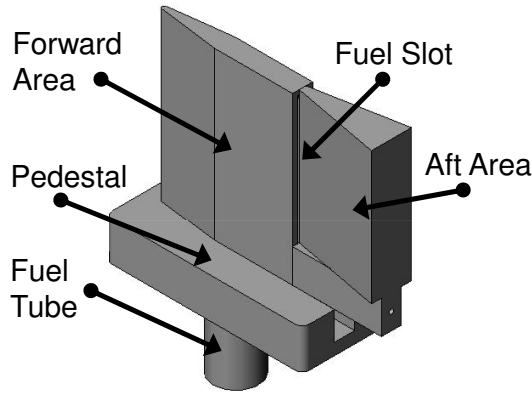
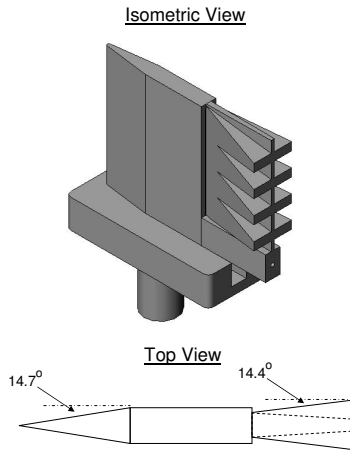

Figure 1. Basic pylon configuration.
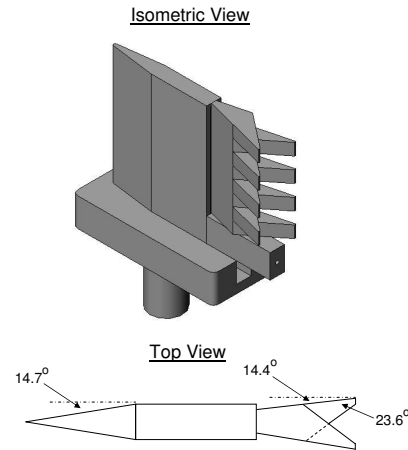

Figure 2. Ramp pylon configuration.

Figure 3. Alternating wedge pylon configuration.

The ramp pylon shown in Fig. 2 includes eight compression ramps on the aft area of the pylon. These compression ramps are 14.4° (half angle) to the main airflow with 8.3° (half angle) of ramp taper (sweep). Past studies have shown that sweep on a hypermixer compression ramp increases streamwise vortices and fuel/air mixing compared with no sweep.[8–10] The compression and sweep angles were chosen to produce the

American Institute of Aeronautics and Astronautics

same frontal blockage area as the basic pylon configuration.

The alternating wedge configuration shown in Fig. 3 includes eight alternating wedges on the aft area of the pylon. Past studies have indicated alternating wedge geometries also produce streamwise vortices and increase fuel/air mixing.[15–17] The wedge geometries have a 23.6° angle and attach to the aft area of the pylon, itself having a 14.4° compression angle (half angle) to the main airflow. This configuration is sized to produce the same frontal blockage area as the other two pylons.

III. Experimental Methodology

Aerothermal probes, Raman spectroscopy, and Planar Laser Induced Florescence (PLIF) are experimental techniques used to measure flow properties in the wake region of these pylons. The different experimental techniques are employed at multiple and overlapping downstream planar positions in the wake region of the pylons. The equivalent diameter, d_e, is the diameter of the geometric, rectangular slot fuel port area if it were to form a circle. The equivalent diameter for the geometric fuel port area (57 mm^2) is 8.52 mm. The planar position downstream of the injection slots is normalized by d_e. The base plane (aft rear face) of each pylon is 40 mm (4.7 d_e) aft of the injection slots.

The nominal flow conditions for the wind tunnel experiments are shown in Table 1. These nominal conditions are based on a momentum flux ratio (Eq. 1) equal to one between the pylon injection gas and the wind tunnel airflow. Note, the effective flow area in Table 1 for the pylons is not the geometric fuel port area. It is the area calculated from mass flow calibration of the pylons. Boundary layers in the fuel port slots cause the effective fuel port area to be slightly smaller than the geometric area.

$$q \equiv \frac{\left(\gamma P M^2\right)_{\text{pylon}}}{\left(\gamma P M^2\right)_{\text{tunnel}}} = \frac{\left(\rho u^2\right)_{\text{pylon}}}{\left(\rho u^2\right)_{\text{tunnel}}} \tag{1}$$

Table 1. Nominal flow conditions for wind tunnel experiments.

Property/Condition	Tunnel Airflow	Pylon Inj (Air)	Pylon Inj (Methane)
Momentum Flux Ratio	–	1.0	1.0
Mass Flux Ratio	–	1.61	1.22
Mach Number	1.95	1.0	1.0
Velocity	501 m/s	311 m/s	411 m/s
Mass Flow	7.14 kg/s	0.031 kg/s	0.023 kg/s
Total Temperature	288 K	288 K	288 K
Static Temperature	164 K	240 K	249 K
Total Pressure	241 KPa	240 KPa	249 KPa
Static Pressure	33.3 KPa	127 KPa	135 KPa
Effective Flow Area	20,129 mm^2	53.7 mm^2	53.7 mm^2

Wind Tunnel

An Air Force Research Laboratory (AFRL) continuous flow supersonic wind tunnel was used for testing.[18] The wind tunnel produced the following conditions for these experiments: 1) Mach number 1.95 and 2) total pressure 241 KPa (35 psi). The test section of the tunnel measured 132.1 mm (5.2 in) high and 152.4 mm (6 in) wide. The length of the test section was approximately 1 m. Optical windows (fused silica) were available for the test section walls during laser experiments, and metal walls were available for probe experiments. Below the test section was a three axis movable table.

Injection gas for the pylon was supplied by high pressure bottles stored outside the facility. The high pressure gas was fed into a regulator that maintained the pressure entering the wind tunnel room at approximately 1.38 MPa (200 psi). A Fairchild® model 10264 precision regulator reduced the pressure to the pylon

American Institute of Aeronautics and Astronautics

injection total pressures from Table 1. Total temperature and total pressure of the pylon injection gas were measured at the output end of the precision regulator just prior to entering the pylon plenum.

Aerothermal Probes

Three probes (thermocouple, cone static, and pitot) were used to measure total temperature, static pressure, and total pressure respectively in the wake region of the pylons. Three separate runs were required to obtain data with the three probes at a single planar position. The wind tunnel test section was configured with one metal sidewall and one window sidewall. The metal sidewall incorporated a slide that traversed in the vertical direction, driven by the three axis table. This allowed for vertical probe movement inside the test section. Horizontal movement of the probe was accomplished using a worm gear drive affixed to the three axis table. The worm gear traverser and movable table worked together to position the probes in the test section and produce two dimensional grids of data at the desired spatial resolution.

A total of 9 cold air pylon injection experiments were accomplished to gather data with the three aerothermal probes in the wake region of the three pylons at one planar position downstream, 23.9 d_e. The probe response times were not fast enough to capture unsteady flow phenomenon, so averaged quantities were obtained. The data acquisition time for a single measurement was 0.5 s for the pressure probes and 1 s for the thermocouple probe. A two dimensional grid of data was constructed at the same array of locations with each probe. Figure 4 shows a cartoon of the probing area location. A 50.8 mm high x 63.5 mm wide (2 in x 2.5 in) array of 189 points was arranged with a 6.35 mm (0.25 in) vertical spacing and 3.175 mm (0.125 in) horizontal spacing. The bottom of the array was 12.7 mm (0.5 in) above the wind tunnel floor, and the middle of the array was centered on the wind tunnel centerline. Local Mach numbers, pressures, densities, and velocities were calculated from probe data.[19] Equation 3 was used to quantify the total pressure loss over the probing area.
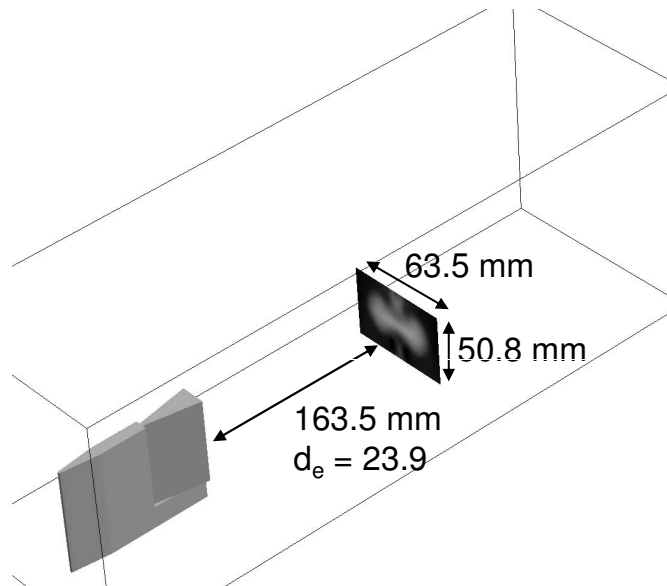

Figure 4. Probing area cartoon.

$$\bar{P}_T = \frac{\int P_T \rho u \, dA}{\int \rho u \, dA} \tag{2}$$

$$\Lambda = 1 - \frac{\bar{P}_T}{P_{T_{\text{tunnel}}}} \tag{3}$$

Raman Spectroscopy

The Raman spectroscopy system used a visible laser beam to interrogate the pylon wake region flowfield.[20, 21] The wind tunnel test section was configured with two window sidewalls and a window top wall for

American Institute of Aeronautics and Astronautics

laser penetration into the test section and camera/spectrometer viewing. The light source was a Coherent®
Verdi laser, a 4.5 Watt continuous source at 532 nm (green). The beam traversed through the test section
at a single height above the floor and single planar position downstream of the pylon. To obtain a two
dimensional profile the beam was incrementally moved to different heights above the tunnel floor during a
single test run using the moveable table. Top and side view diagrams of the Raman setup are shown in Fig.
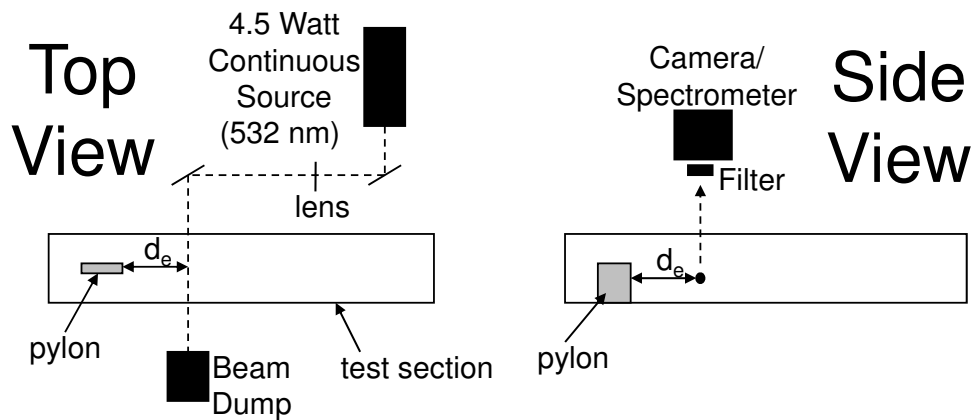5.

Figure 5. Raman experiment setup diagram.

The Raman scattering signals of interest were resultant from the excited vibrational mode of nitrogen
and methane molecules. Each molecular species shifts the frequency of the interrogation light. The shifted
Stokes Raman signal from the methane is at 630 nm. The shifted Stokes Raman signal from the nitrogen
is at 607 nm. Oxygen present in the wind tunnel air also returns a Stokes Raman signal at 580 nm. The
camera/spectrometer equipment used to detect the Raman signals was a Kaiser® Holospec, f/1.8 aperture
size, with an Andor® back-illuminated CCD detector. The spectrometer and CCD camera were configured
to record spectra over a range of approximately 550 nm - 650 nm to capture all the Stokes Raman signals
from the wind tunnel flow and methane injectant. A Schott® Glass OG 570 long-pass filter was placed in
front of the aperture to attenuate the laser light source frequency (532 nm). The spectrometer also acted
as a filter since it was looking in the 550 nm - 650 nm frequency range. Filtering the light source frequency
prevented Rayleigh and Mie scattering signals from overwhelming the Raman scattering signal.

Calibration measurements were accomplished to determine the coefficient curves relating nitrogen and
methane Raman signal intensities to their respective number densities along the 1-D laser beam path in
the test section. A total of 6 Raman experiments were accomplished to gather Raman signal data on all
three pylons at two planar positions downstream of the pylon base plane: 13.6 d_e and 23.9 d_e. At each
height position, the camera shutter opened for 20 s to allow the Raman scattering signals time to integrate,
then the movable table would traverse the laser beam and camera/spectrometer setup to the next height.
A two dimensional grid of data 50.8 mm high x 63.5 mm wide (2 in x 2.5 in) was constructed. The bottom
of the array was 12.7 mm (0.5 in) above the wind tunnel floor, and the middle of the array was centered
on the wind tunnel centerline. The vertical resolution was 3.175 mm (0.125 in). The horizontal resolution
was approximately 0.254 mm (0.01 in), the resolution of the camera/spectrometer images. During data
reduction, the horizontal data was adjusted to 3.175 mm (0.125 in) spacing so the vertical and horizontal
resolutions were comparable when constructing mass fraction profiles.

Background signal was subtracted from the nitrogen and methane signal data and the intensity values
multiplied by their respective calibration curves to determine methane and air number densities. The number
densities were then converted into methane/air mass ratios. The nitrogen signal alone was used to determine
the number density of air present since the ratio of nitrogen to oxygen molecules in air remains constant
in a cold flow. Mass ratios are insensitive to total density changes and window fowling since it is only the
species fractional makeup of the flowfield sought, not absolute quantities. The methane/air mass ratios were
converted into methane mass fractions for plotting results. Mass fraction plume profiles were constructed
in order to determine the diluted state and flammable extent of the methane/air mixture at two planar
positions in the wake region of the pylons.

American Institute of Aeronautics and Astronautics

The amount of mixing occurring at a planar position is represented by the maximum methane mass fraction present in the fuel plume at that position. The maximum mass fraction decreases in the downstream direction as the methane is mixed into the airstream. A smaller maximum methane mass fraction indicates a more mixed fuel plume. The maximum mass fraction is calculated by taking the average of the top 1% of mass fraction values at a planar position in order to guard against a single data outlier.

Mixing effectiveness does not tell the whole story. The amount of mixing is an indicator of how diluted the fuel is in the airstream, but there is a range of flammable mass fractions for a methane/air mixture. If the mass fraction is too high, the mixture is too rich for combustion, and if the mass fraction is too low, the mixture is too lean. Instead of looking at just the mixed state of the fuel plume, it is important to also examine the combustible mixture state. Specifically, how much plume area is combustible at a planar position and what fraction of the total fuel plume area is combustible.

The flammable region is defined using flammability limits. The equivalence ratio flammability limits for methane are $0.53 \leq \phi \leq 1.6$.[22] The stoichiometric methane/air mass ratio, f_s, is approximately 0.058. Consequently, from Eq. 4, the range of flammable mass fractions of methane fuel in air is $0.030 \leq \alpha \leq 0.085$. This is the flammable region.

$$\alpha \;=\; \frac{\phi f_s}{\phi f_s + 1} \tag{4}$$

The flammable plume extent is observed in two quantities. First is the fuel plume area having methane mass fractions within the flammable region. This quantity is normalized by the effective fuel injection area. Second is the fraction of the fuel plume area falling within the flammable region. The first quantity compares the overall flammable plume area between pylons. The second quantity determines the planar position where the fuel plume exhibits the largest fraction of flammable area for each pylon. Figure 6 shows a generic fuel plume cartoon. The shape (circular) is notional, and not realistic. The flammable plume area, FP_a, and the flammable plume fraction, FP_f, are shown in Eqs. 5 and 6. The effective fuel injection area, A_e, is 5.37E-5 m^2. The total fuel plume area, A_p, is defined as the area of fuel plume having mass fractions greater than 0.001.

$$FP_a \;=\; \frac{A_f}{A_e} \tag{5}$$
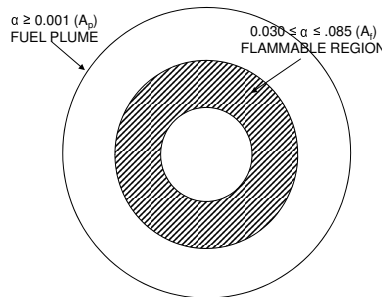
$$FP_f \;=\; \frac{A_f}{A_p} \tag{6}$$

Figure 6. Fuel plume cartoon.

Planar Laser Induced Fluorescence

NO-PLIF as performed here used a laser plane light source to interrogate the pylon wake region flowfield at a ro-vibronic transition frequency of nitric-oxide (NO).[20] The result was a fluorescence signal from the NO. A 1% by volume NO in N_2 seeding gas was added to pylon injection air well upstream of the pylon plenum. Upstream injection allowed the NO to evenly distribute within the injection air. The amount of NO in the total injection mixture was around 0.07% by mass.

The light source was created through a combination of a Spectra Physics® Quanta Ray Nd:YAG laser (GCR-170) and a Lumonics® Hyperdye dye laser (HD-300). The second harmonic of the YAG laser (532 nm) pumped the dye laser, which produced 622 nm radiation. The 622 nm radiation was mixed with the third harmonic of the YAG (355 nm) using a INRAD® Autotracker III and PHS system to produce approximately 226 nm radiation (ultraviolet).

The 226 nm laser beam was distributed into a planar sheet using a planar concave cylindrical lens (-50 mm focal length) and a spherical convex lens (1 m focal length). The two dimensional planar sheet was approximately 100 mm high and was focused at the wind tunnel test section centerline. The laser penetrated one sidewall and was caught by a beam dump after passing through the other sidewall. In this case, unlike the Raman experiments, the camera was viewing from a side angle. The camera was a Roper PIMAX® CCD with a Superblue intensifier, and incorporated a Cerco 45 mm f/1.8 UV lens. The camera was attached to a Scheimpflug mount to mitigate image blur from the off-normal viewing angle. Top and side view diagrams of the NO-PLIF setup are shown in Fig. 7.
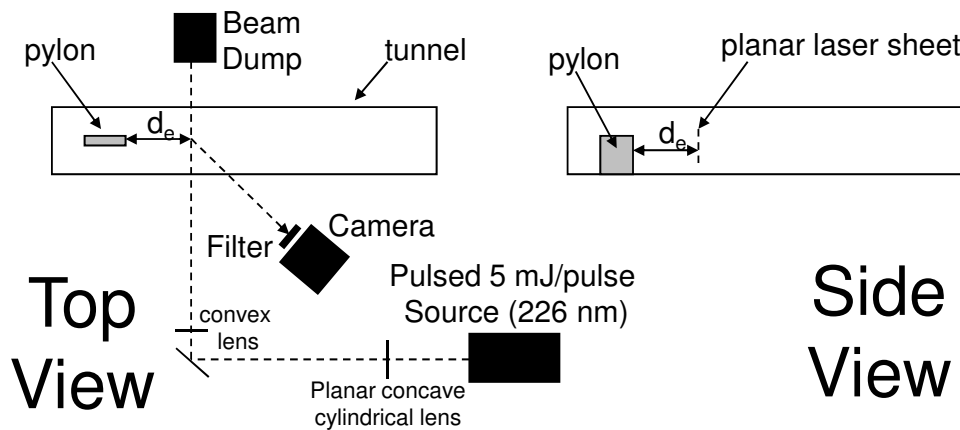

Figure 7. NO-PLIF experiment setup diagram.

The laser configuration was tunable so a precise NO transition could be identified. The NO transition used during experiments was $R_1(8.5)$. The laser was pulsed, having a 10 ns pulse length and a 10 Hz rate. The power output of the laser was 5 mJ per pulse. The camera gate time set to capture the fluorescence signals from the flowfield was 200 ns. A UG 5 band-pass filter was placed in front of the camera lens to reduce Rayleigh and Mie scattering at the frequency of the light source, passing fluorescence signals above 226 nm.

The pulsed laser frequency was not fast enough to capture flow changes at the appropriate time resolution. We obtain temporally resolved images that are uncorrelated (no relation between one another). The fluorescence signal intensities are affected by the temperature and pressure of the local flowfield interrogated due to electronic quenching and collisional line broadening. No temperature or pressure corrections were attempted, so the fluorescent intensity data gathered was qualitative. However, the data still provided comparisons among the pylons and provided excellent flow visualization of the pylon wake regions.

A total of 18 NO-PLIF experiments were accomplished to gather fuel plume signal intensity data on all three pylons at six planar positions downstream of the pylon base plane: 7.7 d_e, 10.7 d_e, 13.6 d_e, 16.6 d_e, 19.6 d_e, and 23.9 d_e. The third and sixth positions, 13.6 d_e and 23.9 d_e, were the same as the Raman experiments; and the sixth position was the same as the probe experiments. For each planar position 300 images were collected over a 30 s period (10 Hz image rate). Ensemble averaged images at each planar position were calculated from the 300 instantaneous images. The averaged images provided mean fuel plume information.

The image perspective distortion was corrected (de-warping) on all images using a MATLAB® projective algorithm prior to any data reduction. Each image was 256 x 256 pixels prior to de-warping, and 346 x 316 pixels after de-warping. The resolution in the vertical and horizontal of the de-warped images is approximately 0.254 mm/pixel (0.01 in/pixel). Just prior to the experiments, background images were taken at each planar position under no wind tunnel flow conditions and no NO present in the test section. Flatfield images were also taken at each planar position under no wind tunnel flow conditions with NO present in the

American Institute of Aeronautics and Astronautics

test section. The background images were subtracted from the data images and the flatfield images were normalized and divided into the data images. The flatfield images were used to help remove laser sheet fluence and window transmission differences within the field of view. However, during testing, substances can build up on the windows and vary the laser sheet pattern slightly in time. The flatfield correction does not account for this.

The final images were cropped to 66.04 mm high x 76.2 mm wide (2.6 in x 3 in) following data reduction. The bottom of the images is 12.7 mm (0.5 in) above the wind tunnel floor, and the middle of the images is centered on the wind tunnel centerline. Signal intensity profiles were constructed in order to visualize the wake region flow of the pylons and determine the diluted state of the mixture at planar positions. The mixing efficiency calculations were accomplished the same way as in the Raman experiments. However, instead of mass fraction data, the top 1% of pixel intensities within the images were averaged and compared among planar positions to observe how quickly the fuel plume is mixed with the airstream.

IV. Experimental Results

Aerothermal Probes

Total pressure loss calculated from pressure and thermocouple probe data at 23.9 d_e reveals at that planar position the basic pylon results in the least pressure loss to the flow and the alternating wedge pylon the most. Compared with the basic pylon, the ramp pylon pressure loss is 9% greater and the alternating wedge pylon pressure loss is 33% greater at that position. Table 2 shows the pressure loss data.

Table 2. Pressure loss comparison at 23.9 d_e.

Pylon	Λ
Basic	0.184
Ramp	0.200
Alternating Wedge	0.244

Mach number profiles constructed using pressure probe data at 23.9 d_e are shown in Figs. 8, 9, and 10. The Mach number profiles for all three pylon at this planar position are supersonic throughout. The shapes of the Mach number profiles is very similar to the fuel plume shapes at the planar position if a fuel were injected instead of air, given equivalent momentum flux ratios. This is observed by comparing the Mach number profiles to fuel plume mass fraction profiles from Raman and NO-PLIF data in Fig. 20. One can use these Mach number profiles as a visual, qualitative assessment of the size and shape of a potential fuel plume. The basic and ramp pylons both exhibit symmetric plume shapes. The alternating wedge pylon plume is asymmetric. This is due to the shape of the aft geometries on the pylons.
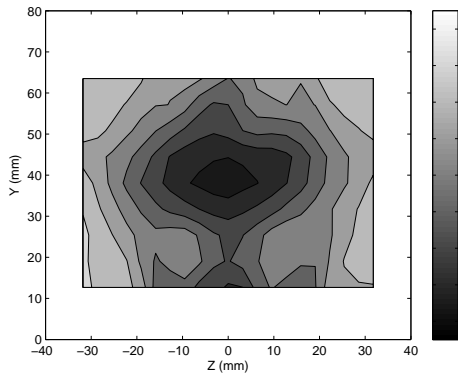

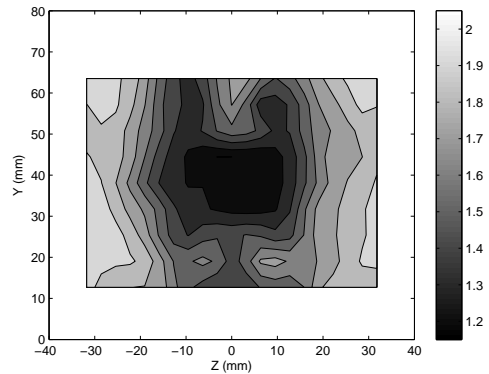Figure 8. Basic pylon mach profile at 23.9 d_e.

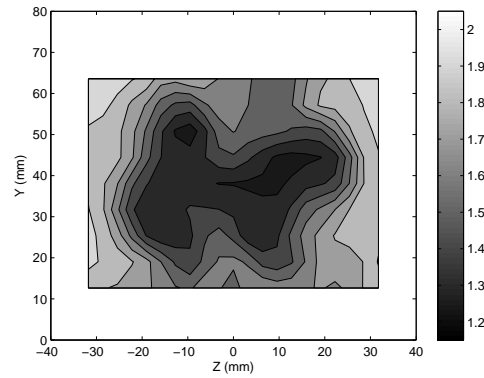Figure 9. Ramp pylon Mach profile at 23.9 d_e.

American Institute of Aeronautics and Astronautics

Figure 10. Alternating wedge pylon Mach profile at 23.9 d_e.

Raman Spectroscopy

Mass fraction profiles constructed using Raman data at 13.6 d_e and 23.9 d_e are shown in Fig. 11. The maximum mass fraction at each planer position for each pylon is shown in Fig. 12. A visual comparison can be made between the mass fraction profiles. Lower mass fractions indicate a better mixed, and therefore more diluted fuel plume. The maximum mass fraction graph gives a quantitative comparison of the pylon mixing performances, using the maximum mass fraction as a measure of mixing.

From a visual comparison using Fig. 11, the mass fractions are smaller at 23.9 d_e than at 13.6 d_e. This is to be expected since the former is farther downstream and has more time to mix with the airstream. At 13.6 d_e, the ramp and alternating wedge pylons result in noticeably lower mass fractions than the basic pylon, with the alternating wedge having the lowest mass fractions. At 23.9 d_e, the alternating wedge pylon is still the most diluted of the three, and the ramp and basic pylons exhibit about the same dilution.

The quantitative comparison of maximum mass fractions in Fig. 12 supports the visual comparisons. The plumes of all three pylons become better mixed progressing downstream. At 13.6 d_e the hypermixer pylons have a more well mixed plume than the basic pylon. At 23.9 d_e there is less overall mixing difference between the pylon plumes, but the alternating wedge is slightly more mixed. From the data it is apparent the vortex production associated with the hypermixer pylons aids mixing in the near-field, but becomes less effective in the downstream region.
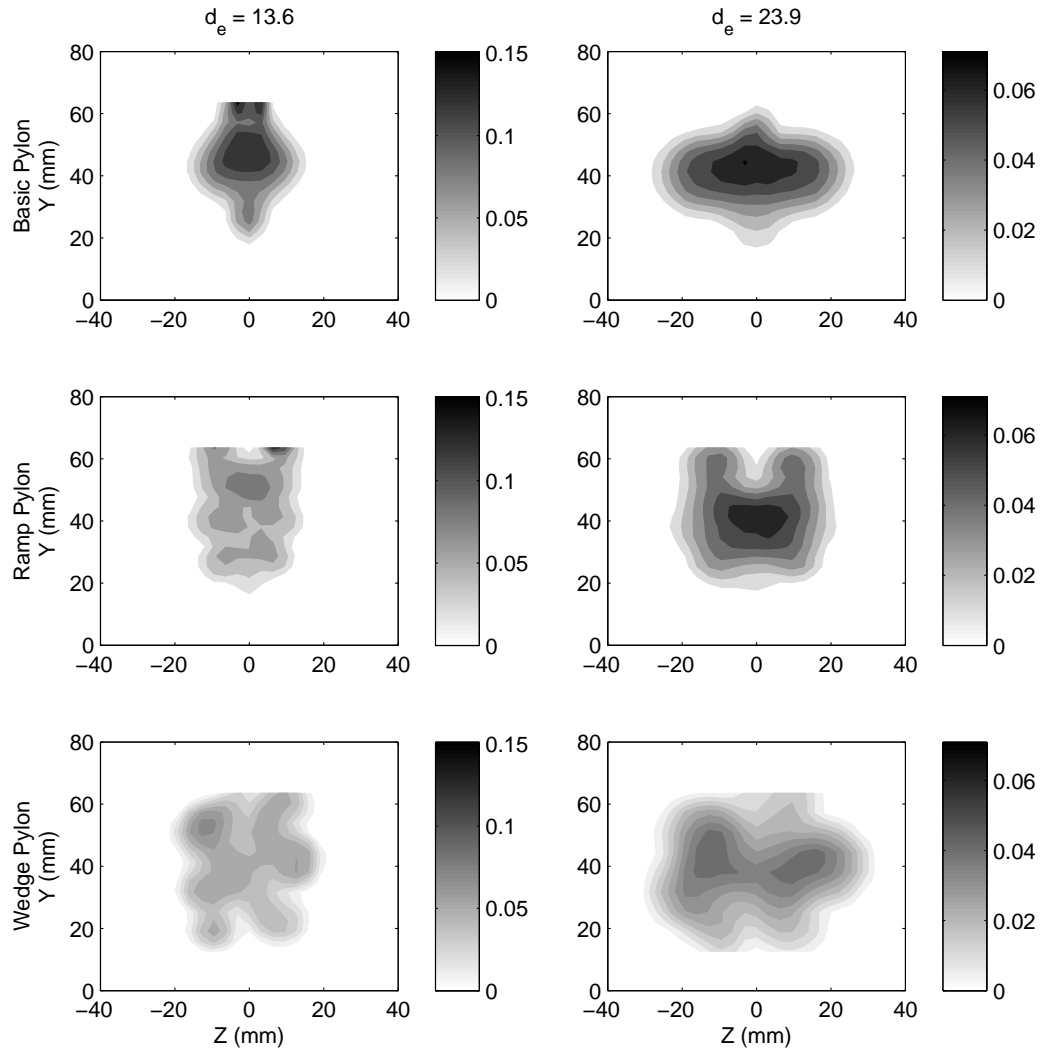
American Institute of Aeronautics and Astronautics

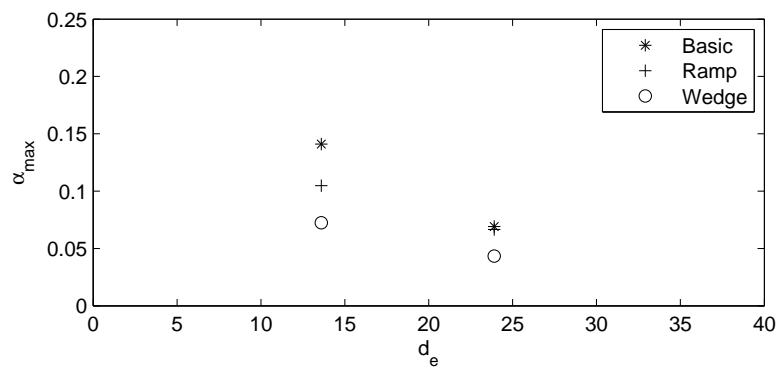**Figure 11. Raman mass fraction profiles.**

Figure 12. Raman maximum mass fraction data.

Figure 13 shows the flammable plume areas and flammable plume fractions for each mass fraction profile. The largest flammable plume area and highest flammable fuel plume fraction are found in the alternating

American Institute of Aeronautics and Astronautics

wedge pylon case at 13.6 d_e. At this planar position about 65% of the methane/air mixture is combustible. At this same planar position the ramp pylon has the second largest flammable plume area/fraction, almost matching the alternating wedge pylon, and the basic pylon has the smallest flammable plume area/fraction. About 25% of the basic pylon plume is flammable at 13.6 d_e.
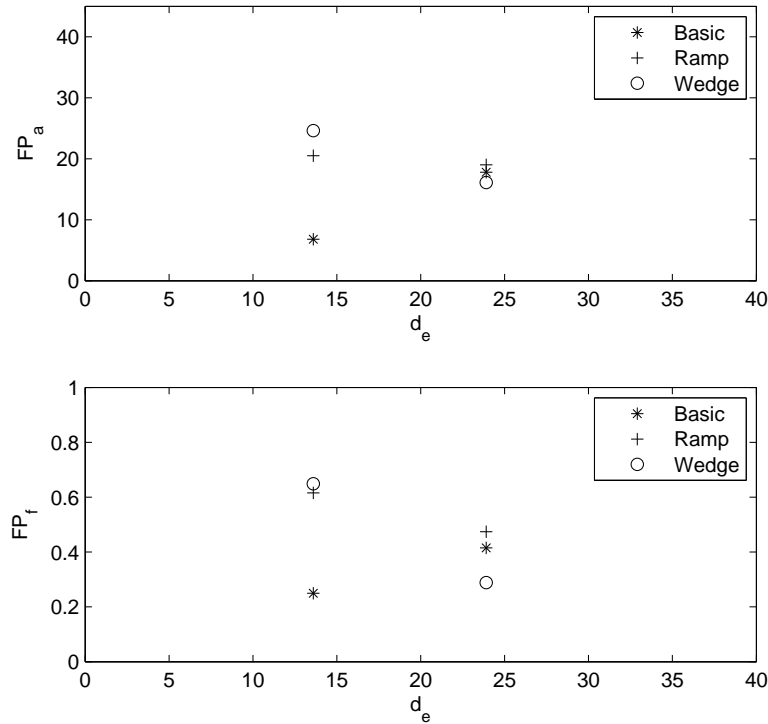

Figure 13. Raman plume flammable area and flammable fraction.

The story is much different at 23.9 d_e. The flammable plume measures from the three pylons are much closer. The alternating wedge has the smallest flammable plume area/fraction, the ramp pylon the largest, and the basic pylon very close to the ramp pylon. The methane/air mixture behind the alternating wedge pylon at this planar position has been diluted so much, many of the local mass fractions have fallen below flammability limits. The ramp pylon flammable plume fraction has fallen off as well at this planar position, but not as much as the alternating wedge pylon. The basic pylon flammable plume area/fraction has increased at 23.9 d_e from 13.6 d_e since many of the local mass fractions above the flammability limit closer to the pylon base plane fall into the flammable region farther away.

These data verify the hypermixer pylons reduce mixing distance downstream of the pylon fuel injector. Between the ramp and alternating wedge pylons, the alternating wedge creates a slightly larger flammable fuel plume and reaches a higher flammable fuel plume fraction in a slightly shorter distance. The mixing differences between the two hypermixer pylons are much less pronounced than the differences between the hypermixer pylons and the basic pylon.

Planar Laser Induced Fluorescence

NO-PLIF data offers instantaneous and ensemble average spatial information about the plume shape in the wake region of the pylons. Figure 14 shows one instantaneous image out of the 300 for each pylon along with the ensemble averaged image of all 300 instantaneous images at 13.6 d_e. The basic pylon plume is highly unsteady, exhibiting side-to-side movement about the centerline of the plume (vortex shedding). An instantaneous image from the basic pylon varies substantially from the ensemble averaged image. An instantaneous image from the ramp and alternating wedge pylons also shows some variation from the ensemble averaged image, but it is much less than the basic pylon. The wake region flow of the two hypermixer pylons is much steadier than that of the basic pylon.
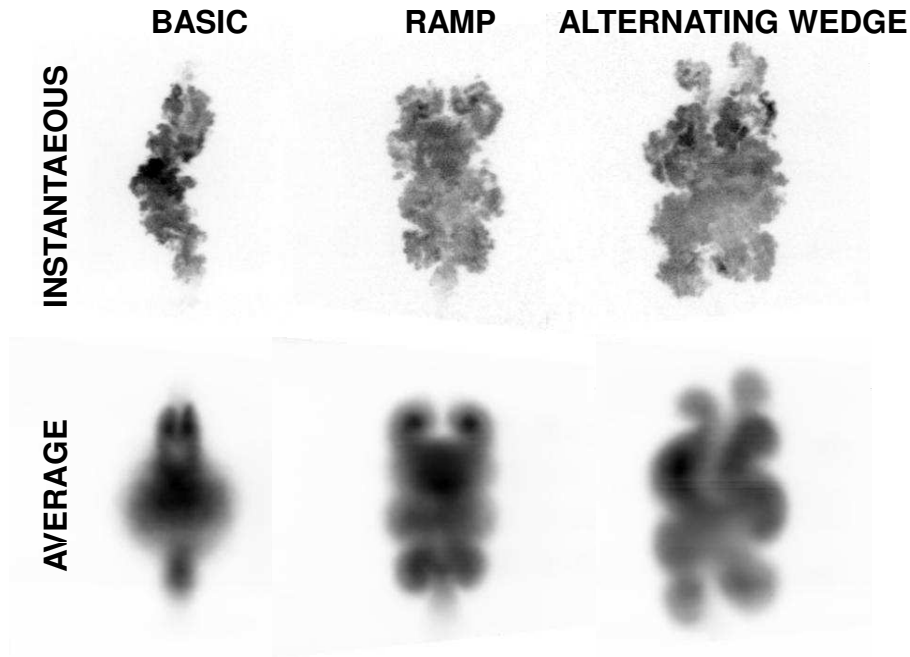
American Institute of Aeronautics and Astronautics

Figure 14. NO-PLIF images at 13.6 d_e.

Figures 15 and 16 show ensemble averaged plume intensity profile images of all three pylons at six planar positions. The pixel intensities of each image are normalized by the maximum pixel intensity present at each respective planar position. The darkest image at a planar position corresponds to the least mixed fuel plume, and the lightest image corresponds to the most well mixed. Since the fuel plume intensity profiles are normalized by planar position, comparison between positions cannot be make with these plots. An attempt was made to globally normalize all fuel plume intensity profiles at all planar positions by the maximum pixel intensity globally, but the mixing rate behind the pylons was rapid enough that the pixel intensities at planar positions farther downstream were too white in the gray scale to be observed visually.

At the three planar positions closest to the pylon base in Fig. 15, the basic pylon has the darkest plume and therefore the least mixed injectant plume of the three. The ramp and alternating wedge pylons are lighter and similar in contrast, indicating they have similar mixed states at these planar positions. At planar positions farther downstream in Fig. 16, there is less of a contrast difference between the three pylon plumes, indicating less of a mixed state difference between the three. At the farthest planar position, 23.9 d_e, the basic and ramp pylons are similar in darkness, indicating their mixed states are similar, while the alternating wedge appears slightly lighter in contrast, indicating a more mixed state than the other two. This is the same trend observed in the Raman data at 13.6 d_e and 23.9 d_e. The ramp and alternating wedge pylons mix the injectant and airstream in a shorter distance, but the basic pylon eventually achieves a similar level of mixing to the hypermixer pylons as downstream distance increases.
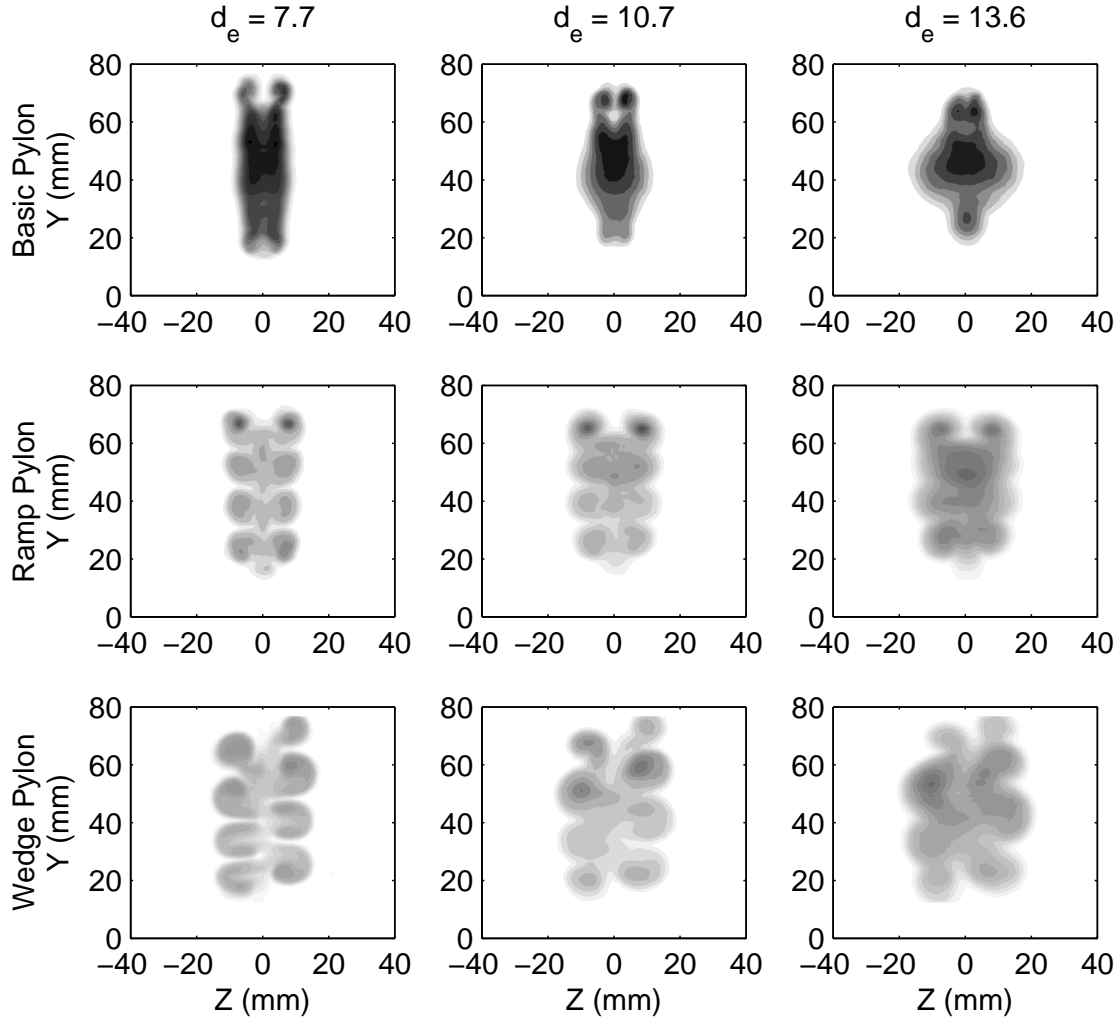
American Institute of Aeronautics and Astronautics

Figure 15. NO-PLIF average plume profiles for 7.7 d_e, 10.7 d_e, and 13.6 d_e.

Although light and dark contrast comparisons cannot be made visually among the planar position in Figs. 15 and 16, the plume shapes can be visually compared among positions. The basic pylon plume close to the pylon base is a long, vertically thin strip of injectant gas. The plume spreads out horizontally and contracts in height as it grows in size with downstream distance. This vertical to horizontal plume shape change is called axis switching. The ramp pylon has tightly concentrated axial vortical structures close to the pylon base plane that help preserve the vertical extent of the ramp plume with downstream distance. The alternating wedge pylon also has intense vortical structures close to the pylon base plane that help preserve the vertical extent of the alternating wedge plume moving downstream. Axis switching is not observed as much in the downstream development of the hypermixer pylons. The axis switching of the basic pylon is mostly a result of the ensemble averaging. The basic pylon instantaneous plume images are shifting left and right across the centerline of the plume due to the vortex shedding. The horizontal extent of the ensemble averaged plume image for the basic pylon is the mean horizontal variation over time. The plume is not actually present in the full horizontal extent at any one instant.
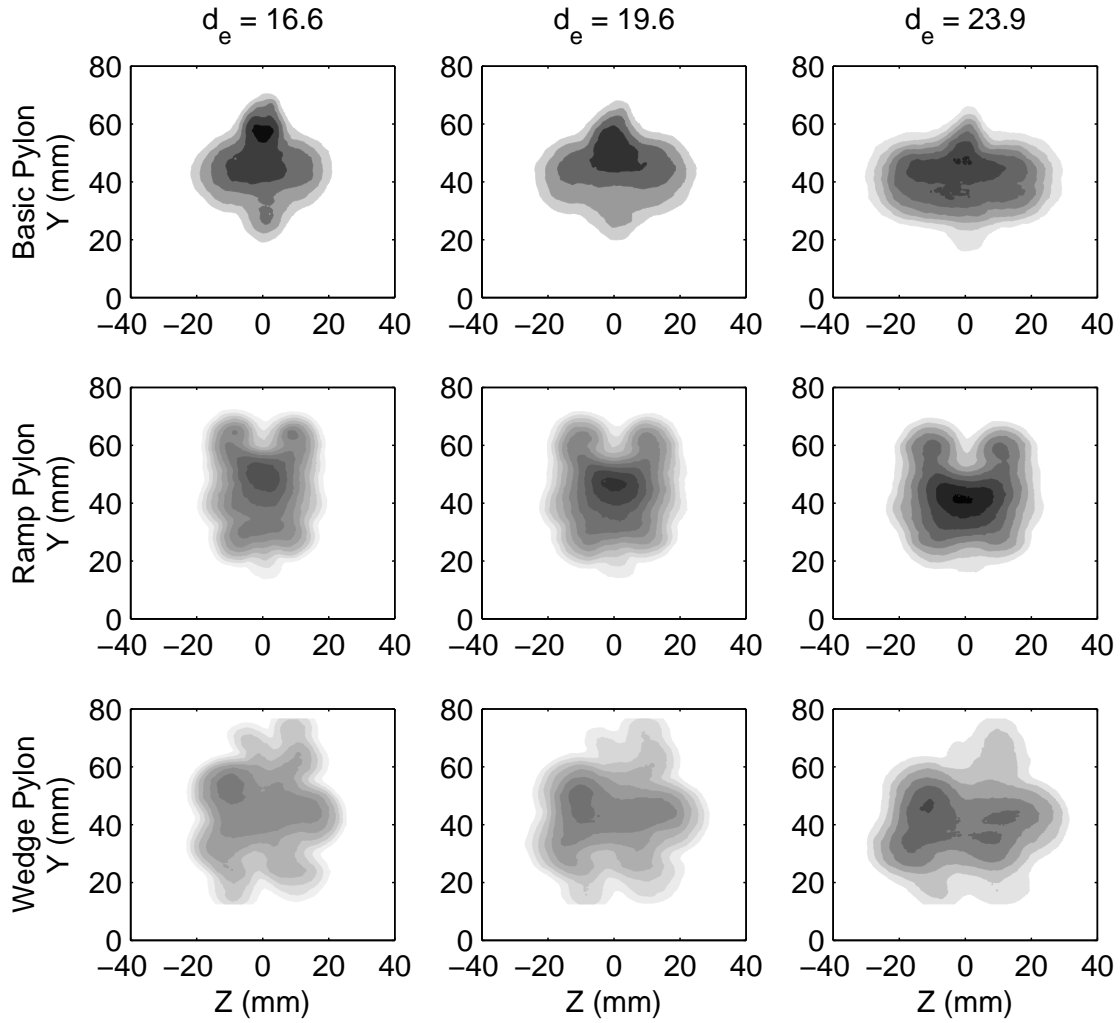
American Institute of Aeronautics and Astronautics

Figure 16. NO-PLIF average plume profiles for 16.6 d_e, 19.6 d_e, and 23.9 d_e.
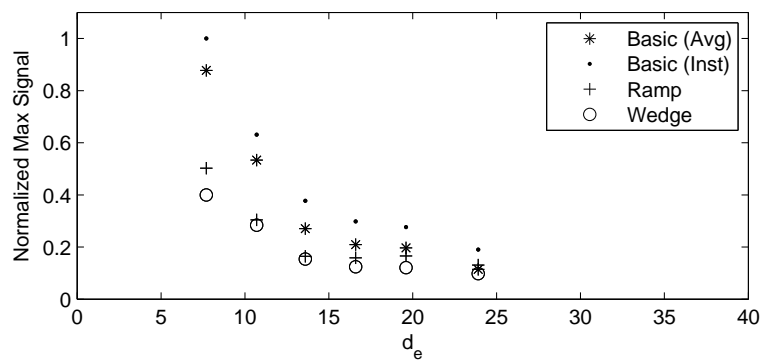

Figure 17. NO-PLIF normalized maximum pixel intensity comparison.

A quantitative comparison of maximum pixel intensity values among planar positions is shown in Fig. 17. The maximum pixel intensities are akin to the maximum mass fraction values in the Raman data. They represent the level of mixing at each planar position. The maximum pixel intensity values in each plume

American Institute of Aeronautics and Astronautics

profile are normalized by the maximum pixel intensity globally at any planar position. The maximum pixel intensity globally is located in the the 7.7 d_e planar intensity profile of the basic pylon. Since all maximum pixel intensities are normalized across the planar positions, comparisons among positions can be made using Fig. 17.

The maximum pixel intensity trends for the pylons match the visual observations of the plume intensity profiles in Figs. 15 and 16. The ramp and alternating wedge pylons mix the injectant into the wind tunnel flow more quickly in the near-field, resulting in lower maximum pixel intensities compared to the basic pylon. However, the basic pylon eventually matches the mixing capability of the hypermixers further downstream. The ramp and alternating wedge pylons are very close in their relative maximum pixel intensities at every planar position, but the alternating wedge does show a slight mixing advantage at most positions.

There is an important distinction to be made between ensemble averaged data and instantaneous data. The ensemble averaged data overestimates the mixed state of the fuel plume compared to the instantaneous data. Fig. 17 displays the maximum pixel intensities for both the ensemble averaged plume intensity profiles as well as the instantaneous plume intensity profiles. The maximum pixel intensities are calculated differently in each case. The maximum pixel intensities for the ensemble averaged profile is accomplished by averaging the top 1% of pixel intensities in the ensemble averaged plume profiles, as stated previously. The maximum pixel intensities for the instantaneous profiles are calculated by averaging the top 1% of pixel intensities in each of the 300 instantaneous images for each planar position, then averaging the 300 maximum intensity values at each position to get a representative maximum pixel intensity value for each position.

If the fuel plumes were perfectly steady, the calculations should be the same. One is the maximum of the instantaneous plume information averaged, and the other is the maximum of the averaged plume information. However, in an unsteady flow, the calculations produce different results. To illustrate the difference, Fig. 18 shows the maximum pixel intensities using the ensemble averaged and instantaneous averaged methods for the three pylons at the six planar positions.

The basic pylon maximum pixel intensity measurements at each position are greater in the instantaneous images than the ensemble averaged image. The ramp and alternating wedge pylons show slight differences between the two as well, but not to the degree seen in the basic pylon. Spatially averaging unsteady flow quantities tends to depress peaks in the data. Since the basic pylon has more unsteadiness in its wake region compared to the hypermixer pylons, the ensemble averaged images overestimate the mixing capability of the basic pylon more so than the hypermixer pylons as seen in Fig. 18.

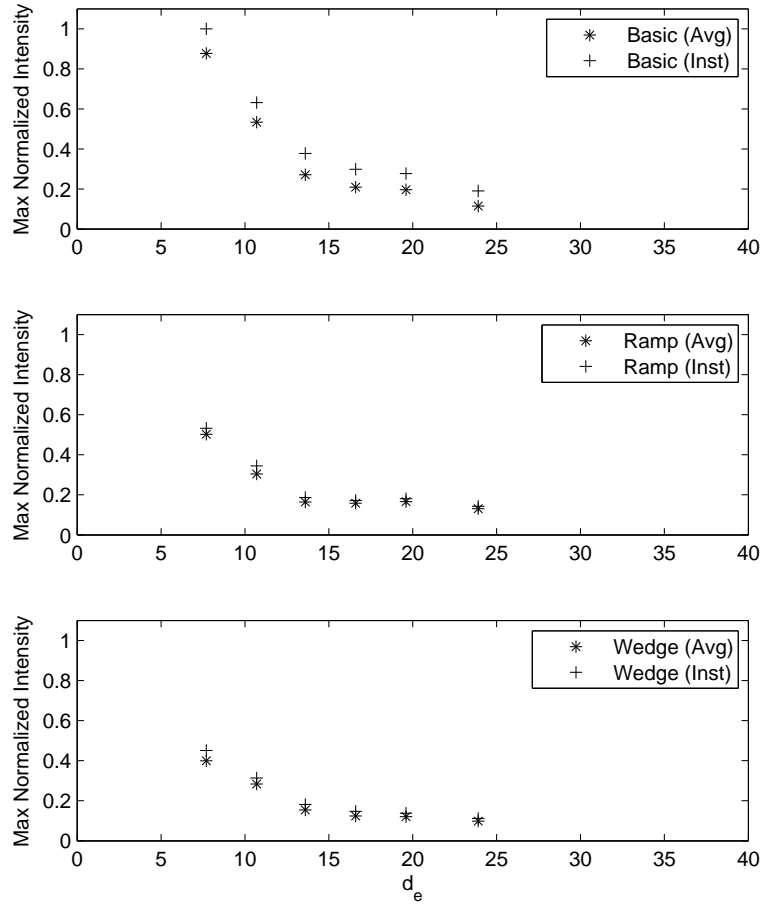American Institute of Aeronautics and Astronautics

Figure 18. NO-PLIF average versus instantaneous image maximum pixel intensities.

The logical question to ask is whether the instantaneous information or the ensemble averaged information is more indicative of the plume's susceptibility to combustion over time. That question cannot be answered by these experiments. Combustion experiments are required. However, the authors believe the instantaneous composition of fuel and air mixtures is a better indication of combustion potential than the ensemble averaged composition of fuel and air because the instantaneous flowfield is where the fuel and air are actually meeting. From the data gathered in the NO-PLIF experiments, ensemble averaged information overestimates the mixing capabilities of a fueled wake region that exhibits highly unsteady flow. It is important to note that the Raman experiments gathered averaged plume information due to the long integration time of the Raman signal. Mass fraction data from those experiments overestimate the basic pylon mixing capability, and to a much lesser degree the hypermixer pylons.

Experimental Technique Comparison

The Raman and NO-PLIF experiments directly measured injectant concentrations and constructed plume profiles. The injectant gases in each case were different. The Raman experiments used methane and the NO-PLIF experiments used air. The momentum flux ratios were kept the same in both cases, but due to the injectant gas differences the mass flux ratios were different. Therefore the amount of mass flow from the pylons in each experiment was slightly different. Data from the Raman experiments is in the form of mass fractions, and data from the NO-PLIF experiments is in the form of signal intensities. The data is normalized for each planar position by the maximum value of the data at that position in each experiment. There were two positions where both Raman and NO-PLIF measurements were collected, 13.6 d_e and 23.9

American Institute of Aeronautics and Astronautics

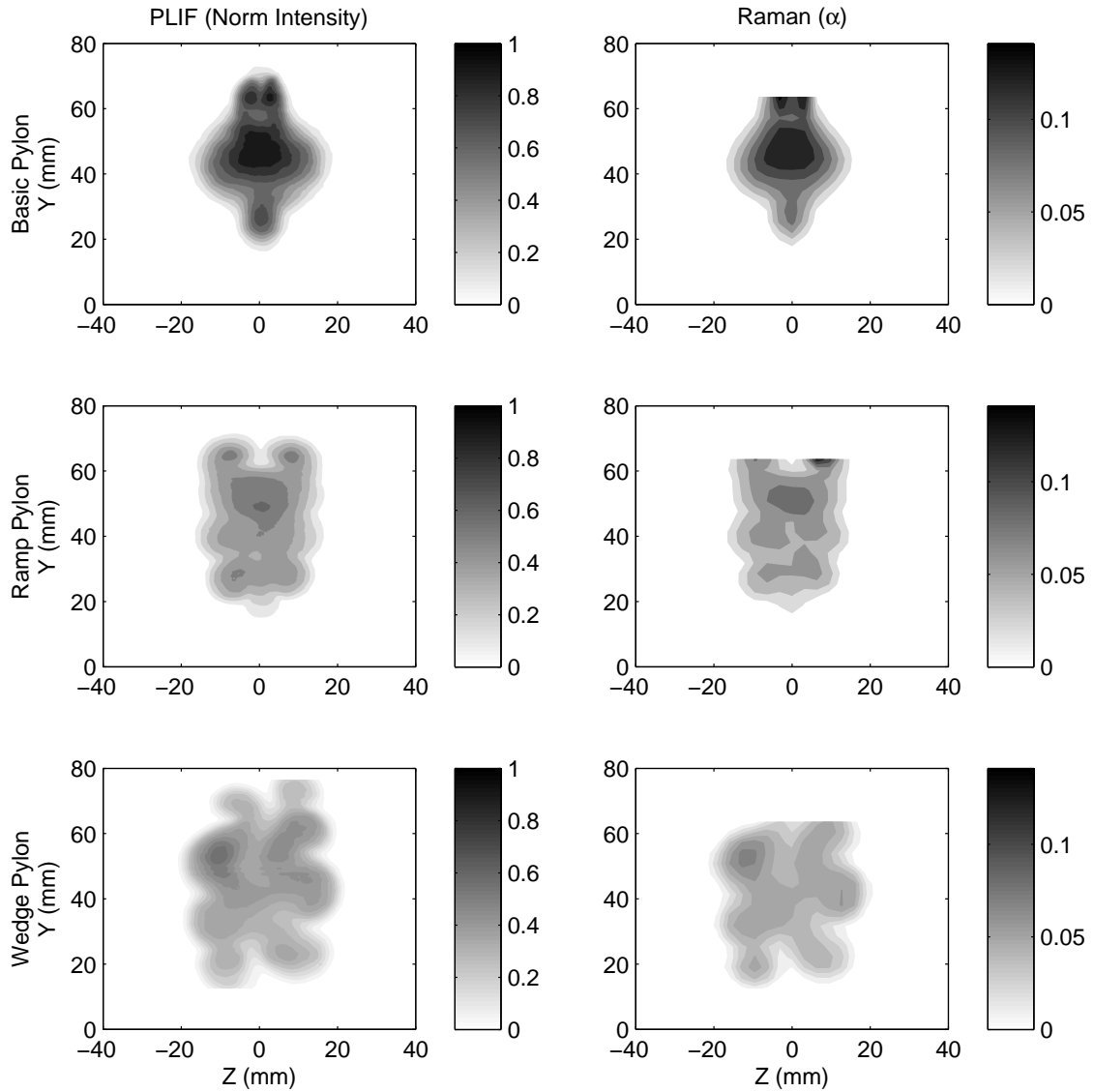d_e. The average plume profile shapes are compared in Figs. 19 and 20.

Figure 19. Raman and NO-PLIF profile comparison at 13.6 d_e.

The plume shapes are similar in using both experimental techniques. There are some intensity distribution differences within the plume boundaries. It is important to point out again that NO-PLIF as it was used here is a qualitative technique. The intensity data depends on more than just the amount of NO present at the location. The data is also affected by temperature and pressure differences within the plume that could not be accounted for since they were not measured simultaneously with the NO-PLIF measurements.

The largest difference between the Raman and NO-PLIF plume profiles is the resolution of each. The Raman data was reduced to 3.175 mm (0.125 in) space intervals and plotted at that resolution in both the vertical and horizontal. The NO-PLIF data was reduced to 0.254 mm (0.01 in) space intervals. The NO-PLIF plume data has an order of magnitude better resolution than the Raman data. This is why the NO-PLIF plume profiles appear slightly larger. The edges of the plume are resolved more finely. Also, in the vertical direction the Raman data was only collected up to 63.5 mm (2.5 in) above the wind tunnel floor, whereas the NO-PLIF data was collected up to 78.7 mm (3.1 in) above the wind tunnel floor. More of the plume vertical extent is captured in the NO-PLIF data.
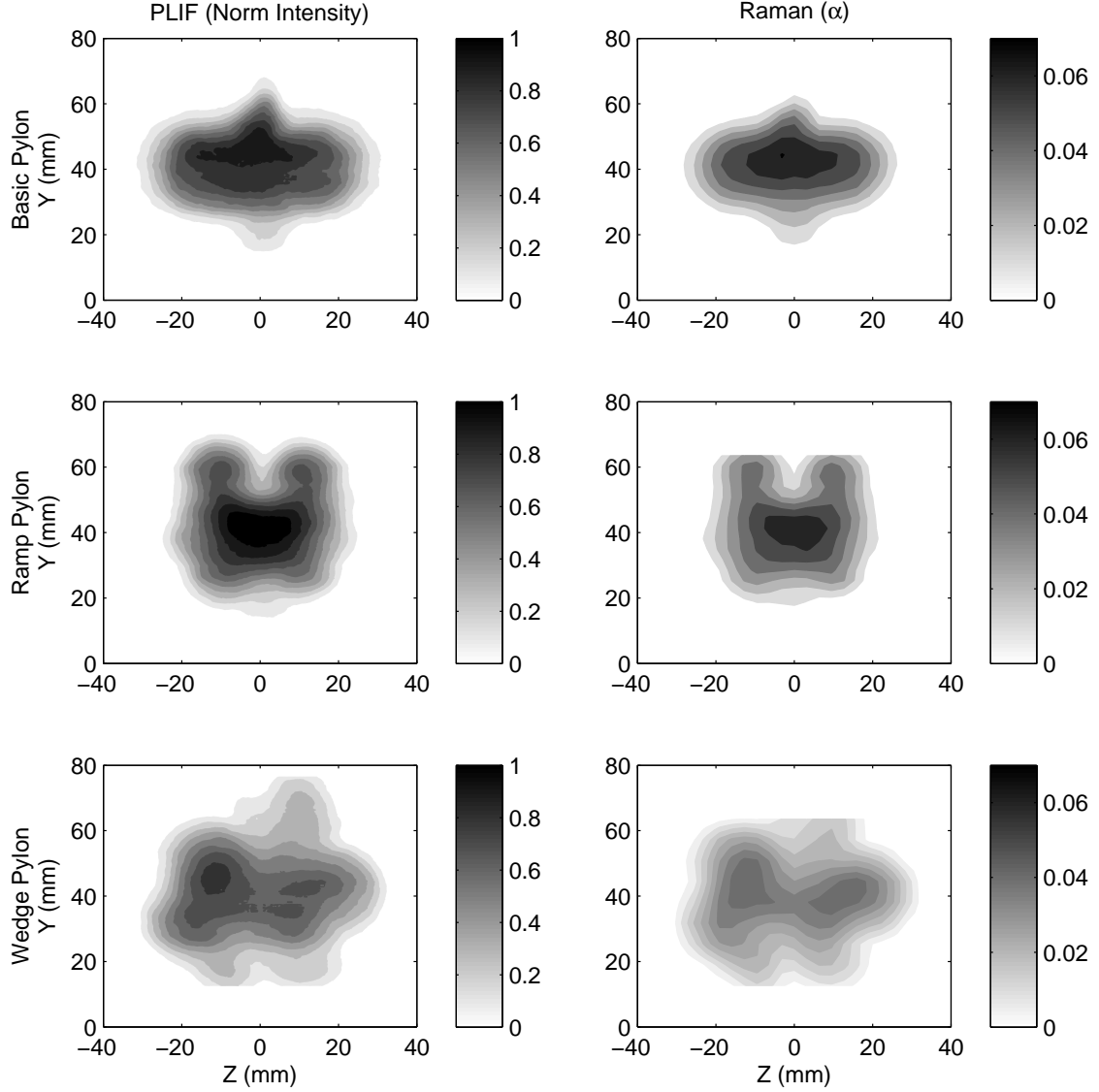
American Institute of Aeronautics and Astronautics

Figure 20. Raman and NO-PLIF profile comparison at 23.9 d_e.

V. Conclusions

The hypermixer pylons exhibit enhanced mixing for a finite distance downstream of the pylon base plane compared with the basic pylon. The length of the enhanced mixing region varies depending on whether averaged data or instantaneous data is observed. Averaged data overestimates the mixing capability of the basic pylon because the wake region flowfield is highly unsteady. The averaged data shows the downstream mixing enhancement distance of the hypermixer pylons over the basic pylon extends to approximately 20 - 25 d_e. The instantaneous data shows the distance extends slightly farther downstream (see Fig. 17). Between the hypermixer pylons, the alternating wedge has a slight mixing advantage over the the ramp pylon.

Mixing capability is not the only important factor when considering the performance of the pylons as fueling devices for a scramjet combustor. Mixing speed determines the distance required to achieve a certain dilution of fuel into the airstream, but there are upper and lower limits of combustible fuel/air mixtures. Fuel plume flammability information is derived from Raman mass fraction data. The mixing enhancement of

American Institute of Aeronautics and Astronautics

the hypermixer pylons moves the combustible mixture region closer to the base plane of the pylon compared to the basic pylon. Between the hypermixer pylons, the alternating wedge exhibits the highest fraction of flammable plume at any position in the wake region. In practice the hypermixer pylons could result in shorter required combustor lengths from reducing the combustion distance. In addition, a combustion flame closer to the pylon base plane where velocities are smaller in magnitude is advantageous for their use as a flameholder.

There are increased pressure losses from the increase in mixing capability. Aerothermal probe data collected at one planar position shows the ramp pylon has 9% more total pressure loss and the alternating wedge pylon 33% more total pressure loss than the basic pylon. The ramp and basic pylons are very close in their total pressure loss. The alternating wedge pylon has a more substantial pressure loss penalty compared to the basic and ramp pylons. Both the hypermixer pylons appear worthy of further study as in-stream scramjet fuel injectors.

The views expressed in this article are those of the authors and do not reflect the official policy or position of the United States Air Force, Department of Defense, or the U.S. Government.

References

[1] *Tam, C., Lin, K., and Raffoul, C., "Review of Jet-in-Crossflow Studies for Scramjet Application," Tech. rep., ARFL/PRAT, Wright Patterson Air Force Base, OH 45433, 2007.*

[2] *Tam, C., Hsu, K., Gruber, M., and Raffoul, C., "Aerodynamic Performance of an Injector Strut for a Round Scramjet Combustor," AIAA Paper 2007-5403, 2007.*

[3] *Doster, J., King, P., Gruber, M., and Maple, R., "Pylon Fuel Injector Design for a Scramjet Combustor," AIAA Paper 2007-5404, 2007.*

[4] *Doster, J., King, P., Gruber, M., and Maple, R., "Numerical Simulation of Ethylene Injection from In-stream Fueling Pylons," AIAA Paper 2008-2518, 2008.*

[5] *Gruber, M., Nejad, A., Chen, T., and Dutton, J., "Transverse Injection from Circular and Elliptical Nozzles into a Supersonic Crossflow,"* Journal of Propulsion and Power, *Vol. 16, No. 3, May-Jun. 2000, pp. 449–457.*

[6] *Heiser, W. and Pratt, D.,* Hypersonic Airbreathing Propulsion, *Education Series, American Institute of Aeronautics and Astronautics, 1994.*

[7] *Curran, E. and Murthy, S.,* Scramjet Propulsion, *Vol. 189 of* Progress in Astronautics and Aeronautics, *American Institute of Aeronautics and Astronautics, 2000.*

[8] *Northam, G., Greenberg, I., and Byington, C., "Evaluation of Parallel Injector Configurations for Supersonic Combustion," AIAA Paper 89-2525, Jul. 1989.*

[9] *Riggins, D., Mekkes, G., McClinton, C., and Drummond, J., "A Numerical Study of Mixing Enhancement in a Supersonic Combustor," AIAA Paper 90-0203, Jan. 1990.*

[10] *Abdel-Salam, T., Tiwari, S., Chaturvedi, S., and Mohieldin, T., "Mixing and Combustion in Scramjet Combustor with Raised and Relieved Ramp," AIAA Paper 2000-3709, Jul. 2000.*

[11] *Kawano, S., Aso, S., and Orino, M., "A Study of a New Injector for Improvement of Supersonic Mixing," AIAA Paper 2000-0089, Jan. 2000.*

[12] *Shreenivasan, O., Kumar, R., Kumar, T., Sujith, R., and Chakravarthy, S., "Mixing in Confined Supersonic Flow Past Strut Based Cavity and Ramps," AIAA Paper 2004-4194, Jul. 2004.*

[13] *Manoharan, S., Chandra, B., Chakravarthy, S., Ramakrishnan, S., and Subramanyam, J., "Experimental Studies of Supersonic Cold Flow Mixing with Ramp Mixers,"* Journal of Aerospace Engineering, *Vol. 18, No. 4, Oct. 2005, pp. 197–205.*

[14] *Aria, T., Sakaue, S., Morisaki, T., Kondo, A., Hiejima, T., and Nishioka, M., "Supersonic Streamwise Vortices Breakdown in a Scramjet Combustor," AIAA Paper 2006-8025, Nov. 2006.*

[15] *Sunami, T., Wendt, M., and Nishioka, M., "Supersonic Mixing and Combustion Control Using Streamwise Vortices," AIAA Paper 1998-3271, Jul. 1998.*

[16] *Sunami, T. and Scheel, F., "Analysis of Mixing Enhancement Using Streamwise Vortices in a Supersonic Combustor by Application of Laser Diagnostics," AIAA Paper 2002-5203, Oct. 2002.*

[17] *Sunami, T., Magre, P., Bresson, A., Grisch, F., Orain, M., and Kodera, M., "Experimental Study of Strut Injectors in a Supersonic Combustor Using OH-PLIF," AIAA Paper 2005-3304, May 2005.*

[18] *Gruber, M. and Nejad, A., "New Supersonic Combustion Research Facility,"* Journal of Propulsion and Power, *Vol. 11, No. 5, Sep.-Oct. 1995, pp. 1080–1083.*

[19] *Fuller, R., Wu, P., Nejad, A., and Schetz, J., "Comparison of Physical and Aerodynamic Ramps as Fuel Injectors in Supersonic Flow,"* Journal of Propulsion and Power, *Vol. 14, No. 2, Mar.-Apr. 1998, pp. 135–145.*

[20] *Eckbreth, A.,* Laser Diagnostics for Combustion Temperature and Species, *Abacus Press, 1988.*

[21] *Demtroder, W.,* Laser Spectroscopy, *Springer, 2003.*

[22] *Glassman, I.,* Combustion, *Academic Press, 1996.*